

Eleven Precursor-Derived Graphene Quantum Dots with Near-Infrared Emission for Bioimaging

by

Himish Paul

Submitted in partial fulfillment of the
requirements for Departmental Honors in
the Department of Physics & Astronomy

Texas Christian University

Fort Worth, Texas

May 5, 2025

Eleven Precursor-Derived Graphene Quantum Dots with Near-Infrared Emission for Bioimaging

Project Approved:

Supervising Professor: Anton Naumov, Ph. D.

Department of Physics & Astronomy

Magnus Rittby, Ph. D.

Department of Physics & Astronomy

Igor Prokhorenkov, Ph. D.

Department of Mathematics

ABSTRACT

Graphene quantum dots (GQDs) have gained attention in the bioimaging community due to their biocompatibility and the capability of some GQDs to facilitate deeply-penetrating near infra-red (NIR) fluorescence image-tracking. Development of multiple NIR fluorescent GQD structures from a variety of precursors can facilitate their application in multiplex imaging, multianalyte sensing and combination therapy delivery. Herein, we demonstrate the synthesis of an unprecedented set of 11 distinct GQD structures capable of NIR fluorescence, achieved through a facile microwave-assisted bottom-up synthesis of 11 different materials: ascorbic acid, chitosan, citric acid, dextran, glucose, glucosamine hydrochloride, hyaluronic acid, l-glutamic acid, polyethylene glycol (PEG), sodium cholate, or sodium citrate. All GQD structures exhibit remarkable biocompatibility at concentrations of up to 2.20 mg/mL and can be successfully tracked by their NIR fluorescence *in vitro* while exhibiting effective cellular internalization in HEK-293 cells . This work provides a unique comprehensive study offering versatility in synthetic approach and physical/chemical properties of biocompatible NIR-emissive GQDs to fit a variety of bioimaging applications.

Table of Contents

INTRODUCTION.....	5
1. MATERIALS AND METHODS	8
<i>1.1. Materials</i>	<i>8</i>
<i>1.2. Microwave-Assisted Synthesis of GQDs</i>	<i>8</i>
<i>1.3. Structural and Optical Characterization</i>	<i>9</i>
<i>1.4. Cell Viability Assays</i>	<i>10</i>
<i>1.5. NIR Fluorescence Imaging.....</i>	<i>10</i>
2. RESULTS AND DISCUSSION	11
3. CONCLUSION	20
4. REFERENCES.....	22

Introduction

Over the past decades, fluorescence imaging has garnered much interest in drug delivery, cellular monitoring, and guided surgery as it is commercially available, sensitive, and non-invasive¹⁻⁵. Fluorescence imaging in the first near-infrared window (NIR-I) (700–900 nm) is well established in the clinical setting due to its minimal absorption attenuation and autofluorescence in biological tissue in comparison to lower wavelengths⁶⁻⁸. This results in greater penetration depth and signal-to-background ratio, making NIR an advantageous region for excitation and emission of fluorescent probes⁶. However, unlike visible fluorophores, their NIR counterparts are scarce, possess lower quantum yields and photostabilities, hindering their wider application in the clinic⁹. This indicates the need in development of NIR fluorophores especially for applications in therapeutic delivery/tracking, multiplex imaging and sensing where fluorophores with different properties can be instrumental.

This niche can be filled by nanoparticles that offer fluorescence imaging and therapeutic transport to the disease site enhanced by targeting or therapeutic modalities such as photothermal and photodynamic therapies^{10, 11}. Therapeutic delivery with real-time tracking allows for precise localization and controlled release of therapeutics, significantly improving treatment efficacy and reducing off-target effects. Such systems are particularly beneficial in cancer therapy, where precise targeting and imaging-guided drug release can enhance the selectivity and effectiveness of treatments, as demonstrated in recent studies involving targeted drug delivery and imaging in glioblastoma¹². Several members of the rapidly expanding family of carbon-based nanomaterials, including graphene oxide, carbon dots, graphene quantum dots, and carbon nanotubes (CNTs), also offer NIR emission capabilities¹³⁻¹⁹. These materials enable simultaneous therapeutic delivery for a wide range of conditions, including prostate, breast, lung, and liver cancers, neurological

disorders, inflammatory diseases, and antimicrobial treatments ²⁰. Functionalized carbon nanotubes (CNTs) can target breast, liver, and prostate cancers through photothermal and gene therapies. While being effective NIR emitters with high photostability, some carbon nanomaterials are associated with toxicity and immunogenicity concerns ^{21, 22} facilitating impairment of mitochondrial function, genetic damage, lysosomal damage, and ultimately, cell death ²³⁻²⁷.

Unlike those, graphene quantum dots (GQDs), have recently been considered one of the least toxic nanoscale materials ²⁸⁻³². The nanoparticles possess exceptional biocompatibility ³³⁻³⁶, high water-solubility ^{37, 38}, exhibit substantial photostability ³⁹⁻⁴² and can perform stand-alone therapeutic functions such as high singlet oxygen generation ⁴³ and photothermal therapy¹⁰, which makes them promising candidates for clinical translation ^{20, 44}. Generally, there are two synthetic means of producing GQDs: the top-down and bottom-up approaches. The top-down method involves the scission of bulk carbonaceous precursors into GQDs with lateral dimensions in the nanometer range ⁴⁵. Cutting of the materials is facilitated by a variety of methods including chemical ⁴⁵⁻⁵⁶, electrochemical ^{44, 57-64}, solvothermal exfoliation ^{31, 47, 65-76}. Further active development of this method features a variety of precursors including graphite ⁷⁷, graphene oxide (GO) ⁷⁸, carbon nanotubes ⁴⁵, coal ⁷⁹, and fullerenes ⁸⁰. None of these structures, however, were reported to exhibit NIR fluorescence. Recently, Hasan et al. (2018) pioneered the use of reduced GO as a precursor for the top-down synthesis of reduced GQDs (rGQDs), which are emissive in the NIR-I with excitation-varying quantum yield of 1-7% ⁷⁸.

As opposed to the top-down method, the bottom-up approach involves the fabrication of nano-sized GQDs from small molecular precursors through hydrothermal, pyrolysis/carbonization, chemical vapor deposition, and electron beam irradiation synthesis procedures ⁸¹. The approach is more scalable and cost-effective as molecular carbonaceous

precursors are abundant. However, the typical photoluminescence of GQDs produced from the bottom-up method is observed in the visible blue/green wavelengths ^{82, 83}. Nevertheless, the bottom-up approach produces GQDs that have more uniform and reproducible structures and sizes than the top-down method ⁸⁴. Pyrolysis is the most straightforward and cost-effective bottom-up technique in which organic material undergoes irreversible thermal decomposition, resulting in carbonization, aromatization, polymerization, and graphitization, which lead to the formation of GQDs ^{85, 86}.

Different GQDs with unique properties may be utilized for specific biomedical applications. Functional groups also aid in different biomedical applications. For instance, amine-functionalized GQDs have shown antimicrobial effects ⁸⁷, ultrastability ⁸⁸ and increased cell entry, which is useful for drug delivery ⁸⁹. Hydroxyl and carboxyl groups enhance the hydrophilicity, promote strong π - π interactions, increase the available surface area, and increase biocompatibility of GQDs ^{85, 90, 91}. However, most bottom-up synthesized GQDs do not exhibit fluorescence in the near-infrared. For biomedical applications, such as non-invasive imaging and targeted drug-delivery, near-infrared fluorescence is key due to high soft tissue penetration depth. Thus, there is a need for a simple, facile synthesis procedure to make GQDs which can be used for such biomedical applications.

In the present work, we utilize the scalability and cost-effectiveness advantages of the bottom-up synthetic approach explored for GQD fabrication, to expand the pool of near-infrared-fluorescing GQD structures and identify the applicability of various precursors specifically for synthesizing GQDS with NIR emission. We assess the optical and structural characteristics of the GQDs using a variety of analytical techniques to elucidate the specific characteristics leading to the formation of the NIR-emissive nanostructures. The bioimaging application is further explored

for biocompatible candidates *in vitro* to validate their further translatability as imaging/delivery agents for a variety of disease targets. The development of such a facile synthetic procedure with a variety of precursor materials for GQDs emitting in the NIR-I region can streamline a wide variety of biomedical applications including multidrug delivery and multianalyte detection.

1. Materials and Methods

1.1. Materials

GQD synthetic precursors included ascorbic acid (Lot #21729, Unpretentious), chitosan (CAS # 84380-01-8, Power Grown), citric acid (CAS #77-92-9, Sigma Aldrich), dextran (CAS # 9004-54-0, Alfa Aesar), glucose (CAS #50-99-7, Innovating Science), glucosamine hydrochloride (Lot #3510840, Millipore Sigma), 5 kDa hyaluronic acid (Part #HA5K-5, Lifecore Biomedical), L-glutamic acid (CAS # 56-86-0, Sigma Aldrich), polyethylene glycol (PEG) (CAS #25322-68-3, Alfa Aesar), sodium cholate (CAS #206986-87-0, Sigma Aldrich), sodium citrate (CAS #6132-04-3, Innovating Science), urea (CAS #57-13-6, Sigma Aldrich), 3-(3,4-Dimethylthiazole-2-yl)-2,5-diphenyl tetrazolium bromide (MTT) (Lot #M6494, Thermo Fisher Scientific), serum-free medium, dimethyl sulfoxide (DMSO).

1.2. Microwave-Assisted Synthesis of GQDs

GQDs were synthesized through heat-treatment of precursor materials in an HB-P90D23AP-ST Hamilton Beach microwave oven. 2.0 grams of precursor, either ascorbic acid, chitosan, citric acid (with 6.0 grams of urea), dextran, glucose, glucosamine hydrochloride, hyaluronic acid, L-glutamic acid, PEG, sodium cholate, or sodium citrate were added into a petri dish and heated in the microwave at 1100W. After 40 to 60 minutes, the organic material darkened, indicating the

formation of GQDs. Once the material cooled to room temperature 50.0 ml of deionized (DI) water was added to disperse the GQDs aided by magnetic stirring for 20 minutes. To purify the product from unreacted precursors, GQDs were dialyzed in 1 kDa dialysis bags against DI water for 24 hours. The water was changed every 30 minutes for the first 3 hours, and then every 7 hours for the next 21 hours. After dialysis, the solutions were syringe-filtered using a 0.22 μm hydrophilic filter membrane to remove aggregates and sterilize. The suspensions were further freeze-dried using a Labconco FreeZone 4.5 freeze dryer for further storage and characterization .

1.3. Structural and Optical Characterization

The morphology, lattice structure, and size distribution of the GQDs were characterized using high-resolution transmission electron microscopy (HRTEM, JEOL JEM-2100). For TEM sample preparation, GQDs are first dispersed in DI, followed by drop-casting onto 300-mesh carbon-coated copper grids. The grids were later dried under ambient conditions prior to imaging. To characterize the functional groups on the GQD surface, the freeze dried samples analyzed using the ATR mode of the Thermo Fisher (Nicolet Nexus 670) Fourier-Transform Infrared Spectrometer (FTIR) in the 500 – 4000 cm^{-1} range. Regions characteristic for most common GQD functional groups were highlighted. The absorbance of all the GQDs was measured between the range of 200 – 1000 nm using a Cary 60 (Agilent Technologies, Santa Clara, CA, USA) spectrometer.

Visible fluorescence spectra of GQDs were evaluated using a NanoLog (HORIBA Scientific, Piscataway, NJ, USA) spectrofluorometer with an excitation wavelength of 400 nm in an emission range of 475 – 700 nm. NIR GQD fluorescence spectra were assessed with AvaSpec-

HS-TEC spectrofluorometer (Avantes, Apeldoorn, The Netherlands) with a 0.9 W/cm² 808 nm laser (808MD-12V-BL, Q-BAIHE, China) excitation.

1.4. Cell Viability Assays

3-(4-dimethylthiazol-2-yl)-2,5-diphenyltetrazolium bromide (MTT) assay was conducted to analyze the biocompatibility of the various GQDs. HEK-293 cells were plated into 96-well plate at a density of 5,000 cells per well and incubated at 37.1 °C with 5% CO₂ for approximately 18 hours. Next, the cells were pre-treated with different concentrations of the GQDs obtained by serial dilutions. After a 24-hour incubation period, the culture medium was replaced with MTT reagent prepared in serum-free medium at a concentration of 1 mg/mL, and the cells were incubated for an additional 4 hours. The MTT solution was then replaced by 100% DMSO to solubilize the formazan crystals, followed by shaking the plates at room temperature for 5 minutes using an orbital shaker. Finally, cell viability was assessed by measuring absorbance at 580 nm using a FLUOstar Omega microplate reader evaluating formazan absorption.

1.5. NIR Fluorescence Imaging

To test cellular uptake of GQDs through NIR fluorescence microscopy, HEK-293 cells were plated onto coverslips positioned in a 6-well plate, with a density of 10,000 cells per well. The coverslips were pre-treated with rat tail collagen I (ALX-522-435-0020, Enzo) according to the manufacturer's instructions to facilitate cell attachment. The following day, GQDs were added to the designated wells at their biocompatible concentrations (Figure 5) and incubated for 12 hours. The coverslips with cells were rinsed using 1X phosphate-buffered saline to remove any GQDs that had not been internalized. To prepare the slides for the NIR fluorescence imaging, the cells were fixed using a 4% formaldehyde solution (Thermo Scientific, 28 908) and mounted with

Fluoromount-GTM mounting medium (Invitrogen, 00-4958-02).

GQDs internalized into the cells were excited with 808 nm laser. Non-internalized GQDs were removed during the washing step. NIR fluorescence microscopy images were taken using an Olympus IX73 fluorescence microscope with a 60 \times (IR-corrected Olympus Plan Apo) water immersion objective. NIR InGaAs Photon etc. (ZephIR 1.7) detector was used to obtain NIR images of GQDs within the HEK-293 cells (850–1600 nm).

2. Results and Discussion

The bottom-up synthetic approach is utilized in this work to produce 11 NIR-emissive GQDs from different precursors: ascorbic acid GQDs, chitosan GQDs, citric acid - urea GQDs, dextran GQDs, glucose GQDs, glucosamine hydrochloride GQDs, hyaluronic acid GQDs, l-glutamic acid GQDs, PEG GQDs, sodium cholate GQDs, and sodium citrate GQDs. The synthesized GQDs are dispersed in deionized (DI) water, followed by dialysis for 24 hours using 1 kDa dialysis membranes against DI water to eliminate unreacted precursors. The purified GQD solution is subsequently sterilized by filtration through 0.22 μm pore-size syringe filters. Transmission electron microscopy (TEM) analysis display GQDs' size distributions for each precursor: (a) Chitosan GQDs 5.63 ± 0.23 nm, (b) Glucosamine Hydrochloride GQDs 5.06 ± 0.99 nm, (c) Ascorbic Acid GQDs 3.13 ± 0.12 nm, (d) Dextran GQDs 4.47 ± 0.25 nm, (e) Sodium Citrate GQDs 3.84 ± 0.93 nm, (f) Sodium Cholate GQDs 3.32 ± 0.17 nm, (g) PEG GQDs 2.81 ± 0.07 nm, (h) L-Glutamic Acid GQDs 3.39 ± 0.11 nm, (i) Hyaluronic Acid GQDs 4.95 ± 0.37 nm, (j) Glucose GQDs 6.63 ± 0.53 nm, and (k) Citric Acid–Urea GQDs 13.47 ± 0.82 nm in diameter. High-resolution transmission electron microscopy (HRTEM) images reveal the graphitic lattice structures in all GQDs, with planar spacings of: (a) Chitosan GQDs 0.37 nm, (b) Glucosamine

Hydrochloride GQDs 0.37 nm, (c) Ascorbic Acid GQDs 0.21 nm, (d) Dextran GQDs 0.21 nm, (e) Sodium Citrate GQDs 0.31 nm, (f) Sodium Cholate GQDs 0.24 nm, (g) PEG GQDs 0.21 nm, (h) L-Glutamic Acid GQDs 0.27 nm, (i) Hyaluronic Acid GQDs 0.34 nm, (j) Glucose GQDs 0.27 nm, and (k) Citric Acid–Urea GQDs 0.27 nm (Figure 1). The crystallinity of GQDs is further confirmed by Fast Fourier Transform (FFT) patterns corresponding to each precursor (Figure 1, insets).

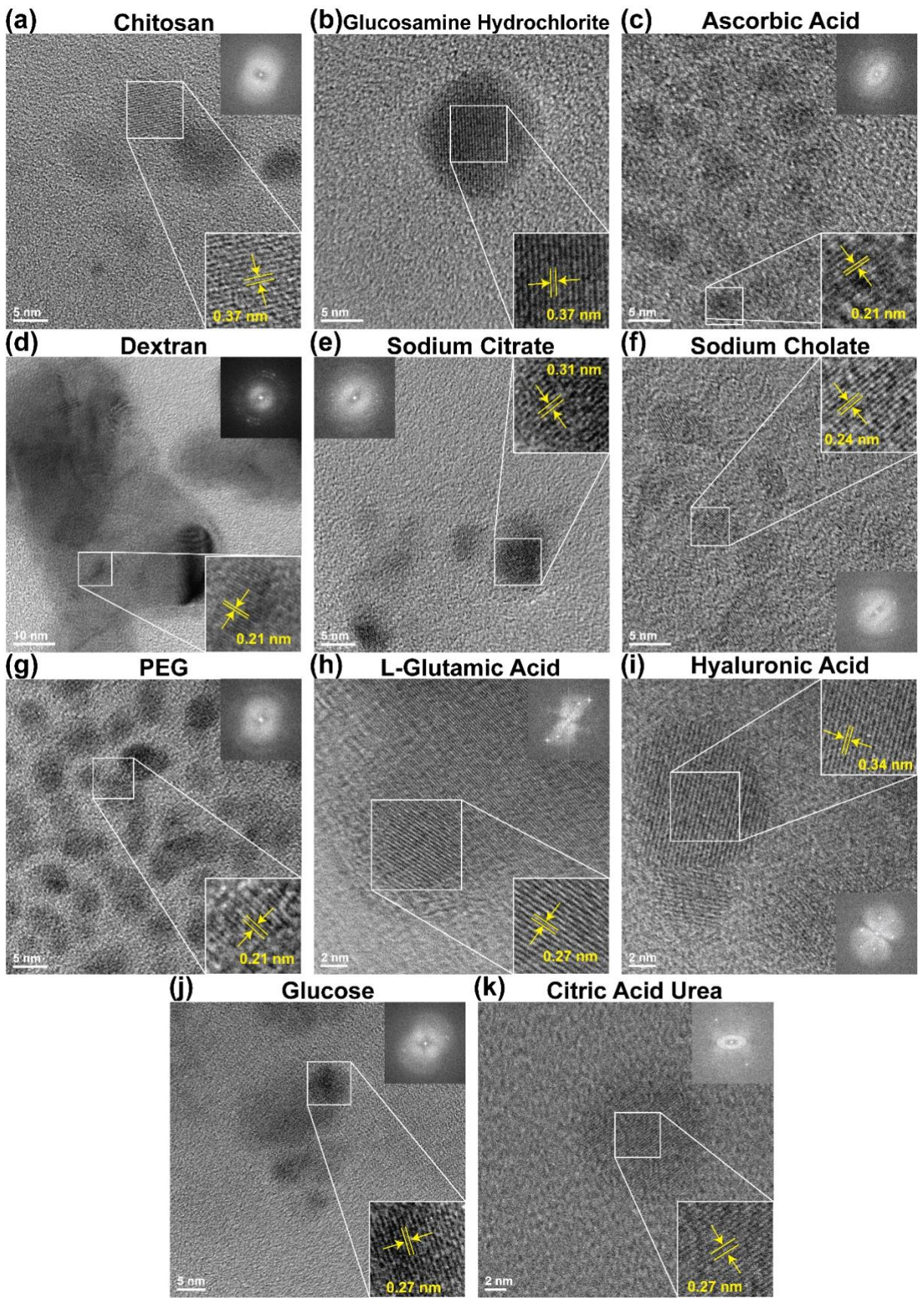


Figure 1: HRTEM images, with insets displaying the interlayer spacings and FFTs of Chitosan GQDs (a), Glucosamine Hydrochloride GQDs (b), Ascorbic Acid GQDs (c), Dextran GQDs (d), Sodium Citrate GQDs (e), Sodium Cholate GQDs (f), PEG GQDs (g), L-Glutamic Acid GQDs (h), Hyaluronic Acid GQDs (i), Glucose GQDs (j) and Citric Acid Urea GQDs (k).

All 11 GQDs possess a number of common functional groups characterized by Fourier Transform Infrared (FTIR) spectroscopy in the ATR mode in freeze-dried GQD samples. Most GQDs have a wide and strong O-H band around 3300 cm^{-1} ⁹² with glucosamine GQDs having a sharper feature PEG-GQDs showing only a weak O-H peak and all GQDs have a C-O peak around $\sim 1060\text{ cm}^{-1}$. Citric acid-urea, hyaluronic acid and l-glutamic acid GQDs all show C-H ($2800\text{--}2920\text{ cm}^{-1}$) stretching bands, and C=O carbonyl stretch ($1560\text{--}1710\text{ cm}^{-1}$) bands which further enhance the solubility of these GQDs in water^{40, 90, 91, 93, 94}. GQDs as aromatic compounds also show aromatic overtones seen as fringes⁹⁵ between $1600\text{--}2000\text{ cm}^{-1}$ with glucosamine hydrochloride displaying only an aromatic C-H band at 3092 cm^{-1} and an aromatic C=C at 1536 cm^{-1} ⁹⁶. The GQDs synthesized from nitrogen-based precursors, possess amine groups: glucosamine GQDs have N-H peaks around 3095 cm^{-1} and 1614 cm^{-1} ⁹⁷ while citric acid-urea GQDs have C-N peaks around 1060 cm^{-1} ⁹⁸. Amine groups enhance the biocompatibility of GQDs by minimizing toxicity, suppressing immune reactions, and promoting smoother integration within biological environments^{85, 99}. Ascorbic acid, citric acid - urea and PEG-GQDs' FTIR spectra indicated a C=O, ester carbonyl group at 1731 cm^{-1} , 1702 cm^{-1} and 1754 cm^{-1} respectively¹⁰⁰ and a C-O group, at 1036 cm^{-1} , 1190 cm^{-1} and 1099 cm^{-1} respectively.

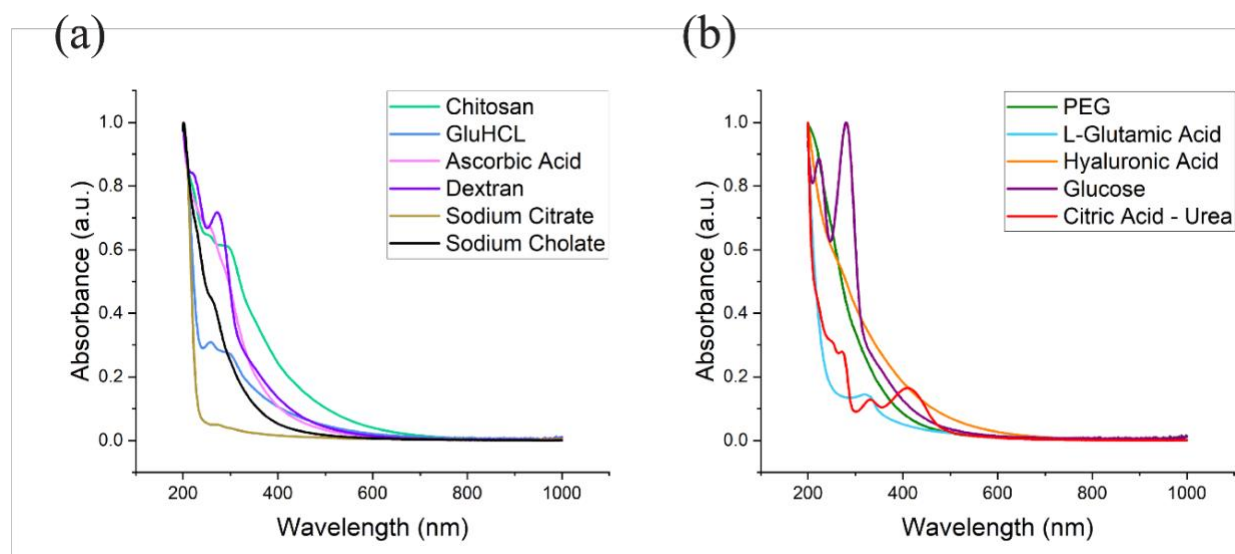


Figure 2: Absorbance spectra of (a) Chitosan GQDs (mint green), Glucosamine Hydrochloride GQDs (blue), Ascorbic Acid GQDs (pink), Dextran GQDs (violet), Sodium Cholate GQDs (dark yellow), and Sodium Cholate GQDs (black) and (b) PEG GQDs (dark green), L-Glutamic Acid GQDs (light -blue), Hyaluronic Acid GQDs (orange), Glucose GQDs (dark purple), and Citric Acid - Urea GQDs (red)

The absorption features of the GQDs further support their structure of oxygenated aromatic nanoparticles revealed in the FTIR imaging (Figure 2). PEG, glucose, dextran, and chitosan GQDs have absorption peaks ~ 220 nm indicating $\pi\text{-}\pi^*$ transition similar to that of C=C bonds in graphene oxide^{101, 102}. Sodium Cholate GQDs have a shoulder in the absorption graph at 264 nm corresponding to their $\pi\text{-}\pi^*$ transition. Peaks between 275 – 300 nm were found in dextran, hyaluronic acid, sodium citrate, citric acid-urea, glucose, glucosamine, and chitosan GQDs arising from the $n\text{-}\pi^*$ transition of the C=O bonds. Chitosan and hyaluronic acid GQDs have long tails that go into the NIR region enhancing their absorption for NIR imaging applications.

Visible fluorescence spectra of the GQDs recorded using a NanoLog spectrofluorometer (HORIBA Scientific, Piscataway, NJ, USA) with 400 nm excitation all show a broad feature within the 475 – 700 nm range. The broad visible emission is attributed to the presence of GQDs with varying sizes within the sample each possessing their distinct set of quantum confinement-defined

excitation and emission wavelengths and altogether amounting to the broad superposition. In contrast, they all show excitation-independent NIR emission (Figure 3) that may arise from localized electronic defects introduced through the incorporation of oxygen-containing functional groups within the graphitic framework.

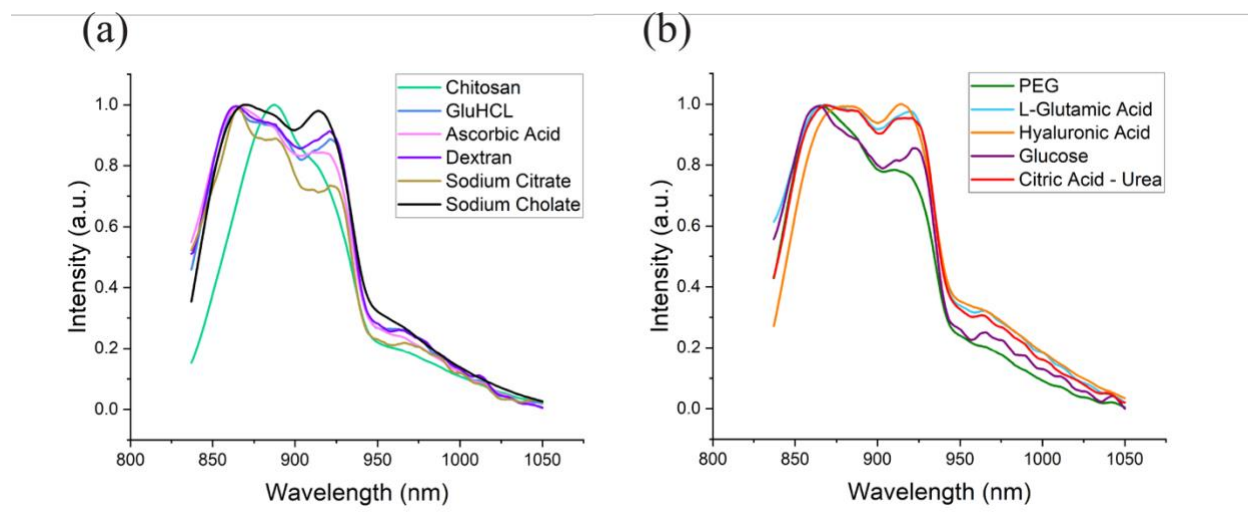


Figure 3: Normalized NIR fluorescence emission of (a) Chitosan GQDs (mint green), Glucosamine Hydrochloride GQDs (blue), Ascorbic Acid GQDs (pink), Dextran GQDs (violet), Sodium Cholate GQDs (dark yellow), and Sodium Cholate GQDs (black) and (b) PEG GQDs (dark green), L-Glutamic Acid GQDs (light-blue), Hyaluronic Acid GQDs (orange), Glucose GQDs (dark purple), and Citric Acid - Urea GQDs (red) with 808 nm excitation.

While most GQDs exhibit a bimodal feature with only chitosan GQDs showing a single NIR peak, the ratios of the peak intensities vary substantially depending on the GQD precursor materials. Thus, while the similarity in the fluorescence graphs tells us that all the GQDs have similar structures, their NIR-emissive defect centers may have different electronic environments resulting in some peak shape/position variations. The NIR GQD emission is critical for biomedical imaging as the NIR light has high soft tissue penetration depths of up to 10 mm¹⁰³.

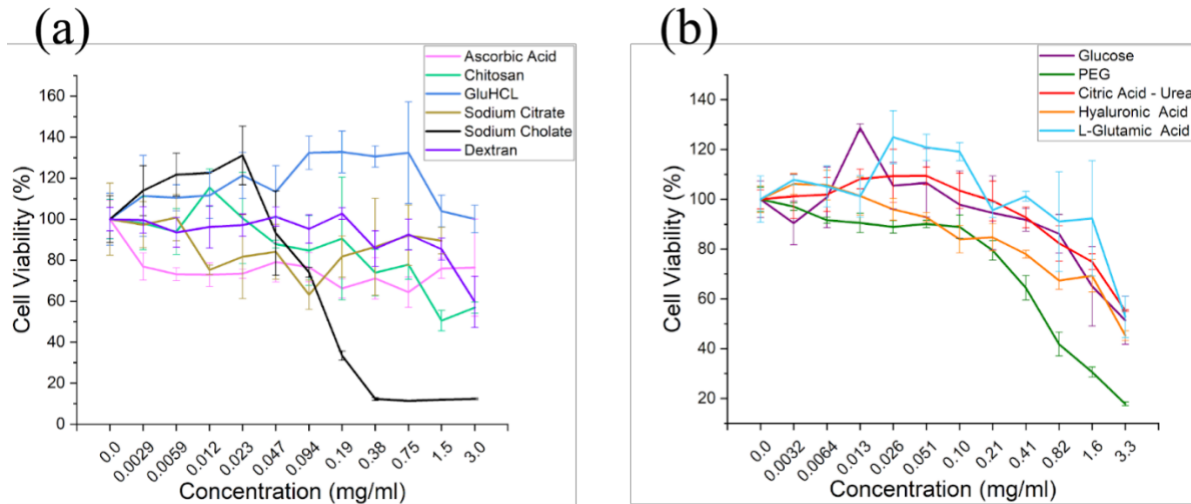


Figure 4: Cell viability of HEK-293 cells treated with (a) Chitosan GQDs (mint green), Glucosamine Hydrochloride GQDs (blue), Ascorbic Acid GQDs (pink), Dextran GQDs (violet), Sodium Cholate GQDs (dark yellow), and Sodium Cholate GQDs (black) and (b) PEG GQDs (dark green), L-Glutamic Acid GQDs (light -blue), Hyaluronic Acid GQDs (orange), Glucose GQDs (dark purple), and Citric Acid - Urea GQDs (red) at different concentrations.

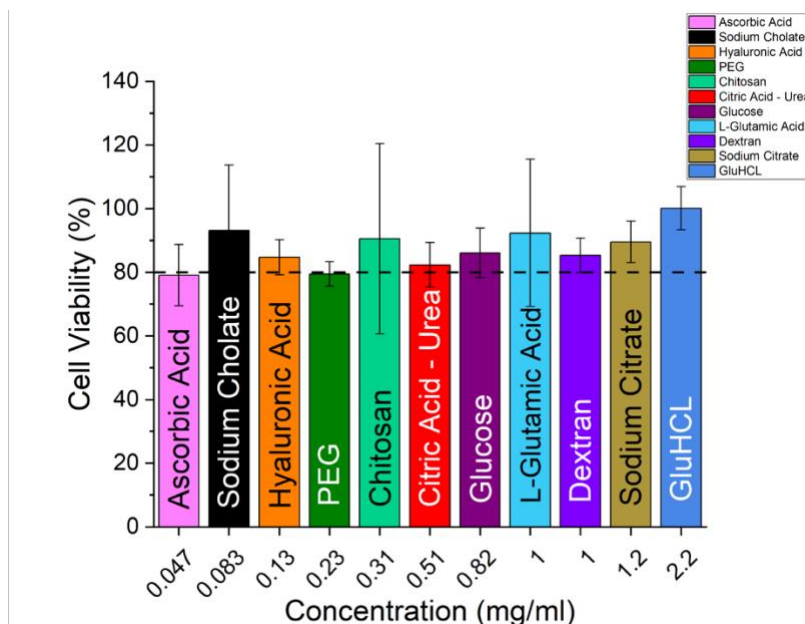


Figure 5: Highest concentration of different GQD types (Chitosan GQDs (mint green), Glucosamine Hydrochloride GQDs (blue), Ascorbic Acid GQDs (pink), Dextran GQDs (violet), Sodium Cholate GQDs (dark yellow), Sodium Cholate GQDs (black), PEG

GQDs (dark green), L-Glutamic Acid GQDs (light -blue), Hyaluronic Acid GQDs (orange), Glucose GQDs (dark purple), and Citric Acid - Urea GQDs (red)) that is biocompatible in cells.

Biocompatibility of the novel imaging agents developed in this work is assessed in HEK-293 cells by the MTT assay (Figure 4) as it is a critical factor for their translation to preclinical applications. Nanomaterials are considered generally biocompatible at above 80% cell viability which is achieved at concentrations between 0.047–2.20 mg/ml with ascorbic acid GQDs showing the lowest and glucosamine hydrochloride GQDs - the highest biocompatible concentrations (Figure 5). These biocompatible concentrations are further used to validate the capabilities of the GQDs for NIR fluorescence imaging *in vitro*.

This is accomplished by tracking GQDs internalized into HEK-293 cells primarily via endocytosis⁹⁷ via their intrinsic NIR fluorescence excited with the 808 nm laser at the maximum GQD internalization time point of 12 hours established in our previous work¹⁰⁴. Since extracellular GQDs are removed in the washing step, there is nearly no emission detected in the extracellular environment with all the GQD NIR fluorescence arising from within the cells (Figure 6). Thus, these eleven GQDs can be used as NIR fluorescence markers.

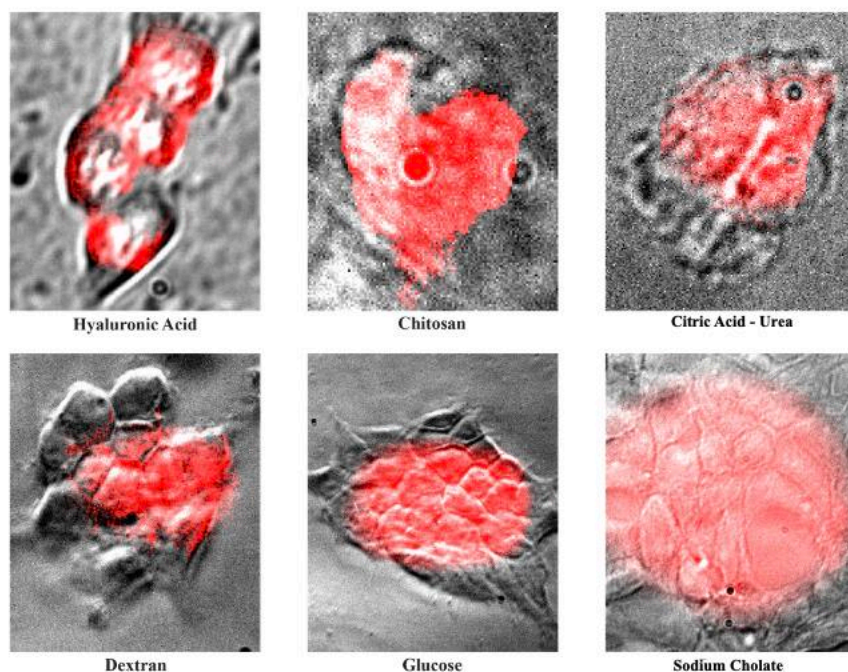


Figure 6: Bright-field and NIR fluorescence overlay of GQD treated cells. Near-infrared GQD fluorescence (shown in red) is excited at 808 nm.

The unique properties of the GQDs synthesized from various precursors uncover their potential for biomedical applications. For instance, different functional groups on their surface can aid in the attachment of therapeutics or targeting agents. For instance, glucosamine and citric acid-urea GQDs, with amine functional groups, can be conjugated with folic acid or peptides for selective targeted uptake cancer cells, enhanced delivery and imaging specificity¹⁰⁵. GQDs bearing oxygen-containing functional groups can be used as pH sensors with their fluorescence affected by protonation and deprotonation of these groups^{29, 106}. Thus the variety of NIR-emissive GQD structures developed in this work offers a broad range of capabilities for enhancing and developing novel biomedical applications of these unique nanomaterials.

3. Conclusion

In this study, we synthesize eleven distinct graphene quantum dot (GQD) structures using a facile, cost-effective, scalable microwave-assisted bottom-up synthesis method from different organic precursors. Structural and optical characterization confirmed the presence of functional groups such as hydroxyl, carboxyl, amine, and ester, which contribute to the GQDs' stability, solubility, and potential for surface functionalization. TEM analysis showed that GQDs synthesized from various precursors exhibited distinct size distributions, ranging from 2.81 ± 0.07 nm (PEG) to 13.47 ± 0.82 nm (citric acid–urea). HRTEM further confirmed their crystallinity, revealing graphitic lattice structures with planar spacings between 0.21 nm and 0.37 nm, supported by corresponding FFT patterns. FTIR spectroscopy demonstrated common functional groups among these GQDs, particularly hydroxyl (O–H), carbonyl (C=O), and ether (C–O) groups, contributing to their enhanced water solubility and biocompatibility. Additionally, nitrogen-containing precursors yielded GQDs with amine groups, known to reduce toxicity, suppress immune reactions, and facilitate integration in biological systems. These GQDs demonstrated visible and NIR fluorescence, water solubility, and substantial biocompatibility at concentrations up to 2.20 mg/mL, making them highly suitable for biomedical applications.

Near-infrared *in vitro* fluorescence microscopy reveals substantial intracellular fluorescence for all 11 GQD structures, indicating efficient cellular internalization of GQDs and supporting their utility in bioimaging applications. The diverse surface functional groups on GQDs provide a versatile platform for targeted drug delivery, pH-responsive sensing, and bio-conjugation with targeting ligands or therapeutic agents.

The findings of this study highlight the tunable physicochemical and biological properties of these novel GQD structures, which can be tailored through precursor selection. This versatility positions them as promising nanomaterials for advanced biomedical technologies, including targeted therapeutics, multimodal imaging, biosensing, and personalized medicine applications. Future studies should focus on evaluating biocompatibility in vivo and exploring translational potential for clinical use.

4. References

- (1) Etrych, T.; Lucas, H.; Janoušková, O.; Chytil, P.; Mueller, T.; Mäder, K. Fluorescence optical imaging in anticancer drug delivery. *Journal of Controlled Release* **2016**, *226*, 168-181.
- (2) Hasan, M. T.; Gonzalez-Rodriguez, R.; Lin, C. W.; Campbell, E.; Vasireddy, S.; Tsedev, U.; Belcher, A. M.; Naumov, A. V. Rare-earth metal ions doped graphene quantum dots for near-ir in vitro/in vivo/ex vivo imaging applications. *Advanced Optical Materials* **2020**, *8* (21), 2000897.
- (3) Lee, B. H.; Hasan, M. T.; Lichthardt, D.; Gonzalez-Rodriguez, R.; Naumov, A. V. Manganese–nitrogen and gadolinium–nitrogen Co-doped graphene quantum dots as bimodal magnetic resonance and fluorescence imaging nanoprobe. *Nanotechnology* **2020**, *32* (9), 095103.
- (4) Lee, B. T.; Hutteman, M.; Gioux, S.; Stockdale, A.; Lin, S. J.; Ngo, L. H.; Frangioni, J. V. The FLARE intraoperative near-infrared fluorescence imaging system: a first-in-human clinical trial in perforator flap breast reconstruction. *Plastic and reconstructive surgery* **2010**, *126* (5), 1472-1481.
- (5) Morgan, N. Y.; English, S.; Chen, W.; Chernomordik, V.; Russo, A.; Smith, P. D.; Gandjbakhche, A. Real time in vivo non-invasive optical imaging using near-infrared fluorescent quantum dots. *Academic Radiology* **2005**, *12* (3), 313-323.
- (6) Zhao, J.; Zhong, D.; Zhou, S. NIR-I-to-NIR-II fluorescent nanomaterials for biomedical imaging and cancer therapy. *Journal of Materials Chemistry B* **2018**, *6* (3), 349-365.
- (7) Hong, G.; Antaris, A. L.; Dai, H. Near-infrared fluorophores for biomedical imaging. *Nature biomedical engineering* **2017**, *1* (1), 0010.
- (8) Chen, G.; Li, C.; Zhang, Y.; Wang, Q. Whole-body fluorescence imaging in the near-infrared window. In *Optical Imaging in Human Disease and Biological Research*, Springer, 2021; pp 83-108.
- (9) Rajendrakumar, S. K.; Chang, N.-C.; Mohapatra, A.; Uthaman, S.; Lee, B.-I.; Tsai, W.-b.; Park, I.-K. A lipophilic ir-780 dye-encapsulated zwitterionic polymer-lipid micellar nanoparticle for enhanced photothermal therapy and nir-based fluorescence imaging in a cervical tumor mouse model. *International journal of molecular sciences* **2018**, *19* (4), 1189.
- (10) Lee, B.; Stokes, G. A.; Valimukhametova, A.; Nguyen, S.; Gonzalez-Rodriguez, R.; Bhaloo, A.; Coffey, J.; Naumov, A. V. Automated approach to in vitro image-guided photothermal therapy with top-down and bottom-up-synthesized graphene quantum dots. *Nanomaterials* **2023**, *13* (5), 805.
- (11) Campbell, E.; Hasan, M. T.; Gonzalez-Rodriguez, R.; Truly, T.; Lee, B. H.; Green, K. N.; Akkaraju, G.; Naumov, A. V. Graphene quantum dot formulation for cancer imaging and redox-based drug delivery. *Nanomedicine: Nanotechnology, Biology and Medicine* **2021**, *37*, 102408.
- (12) Lu, G.; Wang, X.; Li, F.; Wang, S.; Zhao, J.; Wang, J.; Liu, J.; Lyu, C.; Ye, P.; Tan, H. Engineered biomimetic nanoparticles achieve targeted delivery and efficient metabolism-based synergistic therapy against glioblastoma. *Nature Communications* **2022**, *13* (1), 4214.
- (13) Zhang, J.; Boghossian, A. A.; Barone, P. W.; Rwei, A.; Kim, J.-H.; Lin, D.; Heller, D. A.; Hilmer, A. J.; Nair, N.; Reuel, N. F. Single molecule detection of nitric oxide enabled by d(AT)15 DNA adsorbed to near infrared fluorescent single-walled carbon nanotubes. *Journal of the American Chemical Society* **2011**, *133* (3), 567-581.
- (14) Iverson, N. M.; Barone, P. W.; Shandell, M.; Trudel, L. J.; Sen, S.; Sen, F.; Ivanov, V.; Atolia, E.; Farias, E.; McNicholas, T. P. In vivo biosensing via tissue-localizable near-infrared-fluorescent single-walled carbon nanotubes. *Nature nanotechnology* **2013**, *8* (11), 873-880.
- (15) Tao, H.; Yang, K.; Ma, Z.; Wan, J.; Zhang, Y.; Kang, Z.; Liu, Z. In vivo NIR fluorescence imaging, biodistribution, and toxicology of photoluminescent carbon dots produced from carbon nanotubes and graphite. *Small* **2012**, *8* (2), 281-290.

- (16) Liu, Z.; Tabakman, S.; Sherlock, S.; Li, X.; Chen, Z.; Jiang, K.; Fan, S.; Dai, H. Multiplexed five-color molecular imaging of cancer cells and tumor tissues with carbon nanotube Raman tags in the near-infrared. *Nano research* **2010**, *3*, 222-233.
- (17) Barone, P. W.; Baik, S.; Heller, D. A.; Strano, M. S. Near-infrared optical sensors based on single-walled carbon nanotubes. *Nature materials* **2005**, *4* (1), 86-92.
- (18) Sun, X.; Liu, Z.; Welsher, K.; Robinson, J. T.; Goodwin, A.; Zaric, S.; Dai, H. Nano-graphene oxide for cellular imaging and drug delivery. *Nano research* **2008**, *1*, 203-212.
- (19) Luo, Z.; Vora, P. M.; Mele, E. J.; Johnson, A.; Kikkawa, J. M. Photoluminescence and band gap modulation in graphene oxide. *Applied physics letters* **2009**, *94* (11).
- (20) Lee, B.; Gries, K.; Valimukhametova, A. R.; McKinney, R. L.; Gonzalez-Rodriguez, R.; Topkiran, U. C.; Coffey, J.; Akkaraju, G. R.; Naumov, A. V. In vitro prostate cancer treatment via CRISPR-Cas9 gene editing facilitated by polyethyleneimine-derived graphene quantum dots. *Advanced functional materials* **2023**, *33* (48), 2305506.
- (21) Orcin-Chaix, L.; Campidelli, S.; Rondin, L.; Fossard, F.; Bretenaker, F.; Chassagneux, Y.; Voisin, C.; Lauret, J.-S. Photostability of Single-Walled Carbon Nanotubes/Polymer Core-Shell Hybrids as Telecom Wavelength Emitters. *ACS Applied Nano Materials* **2020**, *3* (7), 7291-7296.
- (22) Lettieri, S.; Giordani, S. Carbon Nanomaterials for Deep-Tissue Imaging in the NIR Spectral Window. *Carbon Nanomaterials for Bioimaging, Bioanalysis, and Therapy* **2019**, 87-114.
- (23) Kasai, T.; Umeda, Y.; Ohnishi, M.; Kondo, H.; Takeuchi, T.; Aiso, S.; Nishizawa, T.; Matsumoto, M.; Fukushima, S. Thirteen-week study of toxicity of fiber-like multi-walled carbon nanotubes with whole-body inhalation exposure in rats. *Nanotoxicology* **2015**, *9* (4), 413-422.
- (24) Pulskamp, K.; Diabaté, S.; Krug, H. F. Carbon nanotubes show no sign of acute toxicity but induce intracellular reactive oxygen species in dependence on contaminants. *Toxicology letters* **2007**, *168* (1), 58-74.
- (25) Cui, D.; Tian, F.; Ozkan, C. S.; Wang, M.; Gao, H. Effect of single wall carbon nanotubes on human HEK293 cells. *Toxicology letters* **2005**, *155* (1), 73-85.
- (26) Sayes, C. M.; Gobin, A. M.; Ausman, K. D.; Mendez, J.; West, J. L.; Colvin, V. L. Nano-C60 cytotoxicity is due to lipid peroxidation. *Biomaterials* **2005**, *26* (36), 7587-7595.
- (27) Yuan, X.; Zhang, X.; Sun, L.; Wei, Y.; Wei, X. Cellular toxicity and immunological effects of carbon-based nanomaterials. *Particle and fibre toxicology* **2019**, *16*, 1-27.
- (28) Fasbender, S.; Zimmermann, L.; Cadeddu, R.-P.; Luysberg, M.; Moll, B.; Janiak, C.; Heinzl, T.; Haas, R. The low toxicity of graphene quantum dots is reflected by marginal gene expression changes of primary human hematopoietic stem cells. *Scientific reports* **2019**, *9* (1), 12028.
- (29) Campbell, E.; Hasan, M. T.; Gonzalez Rodriguez, R.; Akkaraju, G. R.; Naumov, A. V. Doped graphene quantum dots for intracellular multicolor imaging and cancer detection. *ACS Biomaterials Science & Engineering* **2019**, *5* (9), 4671-4682.
- (30) Chong, Y.; Ma, Y.; Shen, H.; Tu, X.; Zhou, X.; Xu, J.; Dai, J.; Fan, S.; Zhang, Z. The in vitro and in vivo toxicity of graphene quantum dots. *Biomaterials* **2014**, *35* (19), 5041-5048.
- (31) Zhu, S.; Zhang, J.; Qiao, C.; Tang, S.; Li, Y.; Yuan, W.; Li, B.; Tian, L.; Liu, F.; Hu, R. Strongly green-photoluminescent graphene quantum dots for bioimaging applications. *Chemical communications* **2011**, *47* (24), 6858-6860.
- (32) Nurunnabi, M.; Khatun, Z.; Huh, K. M.; Park, S. Y.; Lee, D. Y.; Cho, K. J.; Lee, Y.-k. In vivo biodistribution and toxicology of carboxylated graphene quantum dots. *ACS nano* **2013**, *7* (8), 6858-6867.
- (33) Zhu, S.; Zhang, J.; Tang, S.; Qiao, C.; Wang, L.; Wang, H.; Liu, X.; Li, B.; Li, Y.; Yu, W. Surface chemistry routes to modulate the photoluminescence of graphene quantum dots: from fluorescence mechanism to up-conversion bioimaging applications. *Advanced Functional Materials* **2012**, *22* (22), 4732-4740.

- (34) Zhang, M.; Bai, L.; Shang, W.; Xie, W.; Ma, H.; Fu, Y.; Fang, D.; Sun, H.; Fan, L.; Han, M. Facile synthesis of water-soluble, highly fluorescent graphene quantum dots as a robust biological label for stem cells. *Journal of materials chemistry* **2012**, *22* (15), 7461-7467.
- (35) Kuo, W.-S.; Chen, H.-H.; Chen, S.-Y.; Chang, C.-Y.; Chen, P.-C.; Hou, Y.-I.; Shao, Y.-T.; Kao, H.-F.; Hsu, C.-L. L.; Chen, Y.-C. Graphene quantum dots with nitrogen-doped content dependence for highly efficient dual-modality photodynamic antimicrobial therapy and bioimaging. *Biomaterials* **2017**, *120*, 185-194.
- (36) Jiang, D.; Chen, Y.; Li, N.; Li, W.; Wang, Z.; Zhu, J.; Zhang, H.; Liu, B.; Xu, S. Synthesis of luminescent graphene quantum dots with high quantum yield and their toxicity study. *PLoS One* **2015**, *10* (12), e0144906.
- (37) Lin, L.; Zhang, S. Creating high yield water soluble luminescent graphene quantum dots via exfoliating and disintegrating carbon nanotubes and graphite flakes. *Chemical communications* **2012**, *48* (82), 10177-10179.
- (38) Kumar, G. S.; Thupakula, U.; Sarkar, P. K.; Acharya, S. Easy extraction of water-soluble graphene quantum dots for light emitting diodes. *Rsc Advances* **2015**, *5* (35), 27711-27716.
- (39) Ma, M.; Hu, X.; Zhang, C.; Deng, C.; Wang, X. The optimum parameters to synthesize bright and stable graphene quantum dots by hydrothermal method. *Journal of Materials Science: Materials in Electronics* **2017**, *28*, 6493-6497.
- (40) Tang, L.; Ji, R.; Cao, X.; Lin, J.; Jiang, H.; Li, X.; Teng, K. S.; Luk, C. M.; Zeng, S.; Hao, J. Deep ultraviolet photoluminescence of water-soluble self-passivated graphene quantum dots. *ACS nano* **2012**, *6* (6), 5102-5110.
- (41) Zhuo, S.; Shao, M.; Lee, S.-T. Upconversion and downconversion fluorescent graphene quantum dots: ultrasonic preparation and photocatalysis. *ACS nano* **2012**, *6* (2), 1059-1064.
- (42) Carrasco, P. M.; García, I.; Yate, L.; Zaera, R. T.; Cabañero, G.; Grande, H. J.; Ruiz, V. Graphene quantum dot membranes as fluorescent sensing platforms for Cr (VI) detection. *Carbon* **2016**, *109*, 658-665.
- (43) Ge, J.; Lan, M.; Zhou, B.; Liu, W.; Guo, L.; Wang, H.; Jia, Q.; Niu, G.; Huang, X.; Zhou, H. A graphene quantum dot photodynamic therapy agent with high singlet oxygen generation. *Nature communications* **2014**, *5* (1), 4596.
- (44) Fan, Z.; Li, Y.; Li, X.; Fan, L.; Zhou, S.; Fang, D.; Yang, S. Surrounding media sensitive photoluminescence of boron-doped graphene quantum dots for highly fluorescent dyed crystals, chemical sensing and bioimaging. *Carbon* **2014**, *70*, 149-156.
- (45) Dong, Y.; Pang, H.; Ren, S.; Chen, C.; Chi, Y.; Yu, T. Etching single-wall carbon nanotubes into green and yellow single-layer graphene quantum dots. *Carbon* **2013**, *64*, 245-251.
- (46) Zhu, C.; Yang, S.; Wang, G.; Mo, R.; He, P.; Sun, J.; Di, Z.; Kang, Z.; Yuan, N.; Ding, J. A new mild, clean and highly efficient method for the preparation of graphene quantum dots without by-products. *Journal of Materials Chemistry B* **2015**, *3* (34), 6871-6876.
- (47) Shin, Y.; Park, J.; Hyun, D.; Yang, J.; Lee, J.-H.; Kim, J.-H.; Lee, H. Acid-free and oxone oxidant-assisted solvothermal synthesis of graphene quantum dots using various natural carbon materials as resources. *Nanoscale* **2015**, *7* (13), 5633-5637.
- (48) Nair, R. V.; Thomas, R. T.; Sankar, V.; Muhammad, H.; Dong, M.; Pillai, S. Rapid, acid-free synthesis of high-quality graphene quantum dots for aggregation induced sensing of metal ions and bioimaging. *ACS omega* **2017**, *2* (11), 8051-8061.
- (49) Kundu, S.; Ghosh, S.; Fralade, M.; Narayanan, T.; Pillai, V. K.; Talapatra, S. Fractional photo-current dependence of graphene quantum dots prepared from carbon nanotubes. *Physical Chemistry Chemical Physics* **2015**, *17* (38), 24566-24569.
- (50) Maiti, S.; Kundu, S.; Roy, C. N.; Das, T. K.; Saha, A. Synthesis of excitation independent highly luminescent graphene quantum dots through perchloric acid oxidation. *Langmuir* **2017**, *33* (51), 14634-14642.

- (51) Kwon, W.; Kim, Y.-H.; Lee, C.-L.; Lee, M.; Choi, H. C.; Lee, T.-W.; Rhee, S.-W. Electroluminescence from graphene quantum dots prepared by amidative cutting of tattered graphite. *Nano letters* **2014**, *14* (3), 1306-1311.
- (52) Shen, J.; Zhu, Y.; Chen, C.; Yang, X.; Li, C. Facile preparation and upconversion luminescence of graphene quantum dots. *Chemical communications* **2011**, *47* (9), 2580-2582.
- (53) Xu, H.; Zhou, S.; Xiao, L.; Wang, H.; Li, S.; Yuan, Q. Fabrication of a nitrogen-doped graphene quantum dot from MOF-derived porous carbon and its application for highly selective fluorescence detection of Fe³⁺. *Journal of Materials Chemistry C* **2015**, *3* (2), 291-297.
- (54) Zhao, P.; Yang, M.; Fan, W.; Wang, X.; Tang, F.; Yang, C.; Dou, X.; Li, S.; Wang, Y.; Cao, Y. Facile one-pot conversion of petroleum asphaltene to high quality green fluorescent graphene quantum dots and their application in cell imaging. *Particle & Particle Systems Characterization* **2016**, *33* (9), 635-644.
- (55) Peng, J.; Gao, W.; Gupta, B. K.; Liu, Z.; Romero-Aburto, R.; Ge, L.; Song, L.; Alemany, L. B.; Zhan, X.; Gao, G. Graphene quantum dots derived from carbon fibers. *Nano letters* **2012**, *12* (2), 844-849.
- (56) Ye, R.; Xiang, C.; Lin, J.; Peng, Z.; Huang, K.; Yan, Z.; Cook, N. P.; Samuel, E. L.; Hwang, C.-C.; Ruan, G. Coal as an abundant source of graphene quantum dots. *Nature communications* **2013**, *4* (1), 2943.
- (57) Huang, H.; Yang, S.; Li, Q.; Yang, Y.; Wang, G.; You, X.; Mao, B.; Wang, H.; Ma, Y.; He, P. Electrochemical cutting in weak aqueous electrolytes: the strategy for efficient and controllable preparation of graphene quantum dots. *Langmuir* **2018**, *34* (1), 250-258.
- (58) Ahirwar, S.; Mallick, S.; Bahadur, D. Electrochemical method to prepare graphene quantum dots and graphene oxide quantum dots. *ACS omega* **2017**, *2* (11), 8343-8353.
- (59) Li, Y.; Liu, H.; Liu, X.-q.; Li, S.; Wang, L.; Ma, N.; Qiu, D. Free-radical-assisted rapid synthesis of graphene quantum dots and their oxidizability studies. *Langmuir* **2016**, *32* (34), 8641-8649.
- (60) Su, Z.; Shen, H.; Wang, H.; Wang, J.; Li, J.; Nienhaus, G. U.; Shang, L.; Wei, G. Motif-designed peptide nanofibers decorated with graphene quantum dots for simultaneous targeting and imaging of tumor cells. *Advanced Functional Materials* **2015**, *25* (34), 5472-5478.
- (61) Tan, X.; Li, Y.; Li, X.; Zhou, S.; Fan, L.; Yang, S. Electrochemical synthesis of small-sized red fluorescent graphene quantum dots as a bioimaging platform. *Chemical Communications* **2015**, *51* (13), 2544-2546.
- (62) Ananthanarayanan, A.; Wang, X.; Routh, P.; Sana, B.; Lim, S.; Kim, D. H.; Lim, K. H.; Li, J.; Chen, P. Facile synthesis of graphene quantum dots from 3D graphene and their application for Fe³⁺ sensing. *Advanced Functional Materials* **2014**, *24* (20), 3021-3026.
- (63) Li, Y.; Zhao, Y.; Cheng, H.; Hu, Y.; Shi, G.; Dai, L.; Qu, L. Nitrogen-doped graphene quantum dots with oxygen-rich functional groups. *Journal of the American Chemical Society* **2012**, *134* (1), 15-18.
- (64) Zhou, S.; Xu, H.; Gan, W.; Yuan, Q. Graphene quantum dots: recent progress in preparation and fluorescence sensing applications. *RSC advances* **2016**, *6* (112), 110775-110788.
- (65) Boonta, W.; Talodthaisong, C.; Sattayaporn, S.; Chaicham, C.; Chaicham, A.; Sahasithiwat, S.; Kangkaew, L.; Kulchat, S. The synthesis of nitrogen and sulfur co-doped graphene quantum dots for fluorescence detection of cobalt (II) ions in water. *Materials Chemistry Frontiers* **2020**, *4* (2), 507-516.
- (66) Qi, B.-P.; Zhang, X.; Shang, B.-B.; Xiang, D.; Zhang, S. Solvothermal tuning of photoluminescent graphene quantum dots: from preparation to photoluminescence mechanism. *Journal of Nanoparticle Research* **2018**, *20*, 1-9.
- (67) Tian, R.; Zhong, S.; Wu, J.; Jiang, W.; Shen, Y.; Wang, T. Solvothermal method to prepare graphene quantum dots by hydrogen peroxide. *Optical Materials* **2016**, *60*, 204-208.

- (68) Wang, G.; Guo, Q.; Chen, D.; Liu, Z.; Zheng, X.; Xu, A.; Yang, S.; Ding, G. Facile and highly effective synthesis of controllable lattice sulfur-doped graphene quantum dots via hydrothermal treatment of durian. *ACS applied materials & interfaces* **2018**, *10* (6), 5750-5759.
- (69) Yu, J.; Liu, S.; Chen, S.; Wang, T. Simultaneous preparation of mesoporous/macroporous graphene aerogels and bright green photoluminescent graphene quantum dots by a simple solvothermal method. *Industrial & Engineering Chemistry Research* **2017**, *56* (36), 10028-10035.
- (70) Chen, W.; Li, D.; Tian, L.; Xiang, W.; Wang, T.; Hu, W.; Hu, Y.; Chen, S.; Chen, J.; Dai, Z. Synthesis of graphene quantum dots from natural polymer starch for cell imaging. *Green chemistry* **2018**, *20* (19), 4438-4442.
- (71) Cirone, J.; Ahmed, S. R.; Wood, P. C.; Chen, A. Green synthesis and electrochemical study of cobalt/graphene quantum dots for efficient water splitting. *The Journal of Physical Chemistry C* **2019**, *123* (14), 9183-9191.
- (72) Halder, A.; Godoy-Gallardo, M.; Ashley, J.; Feng, X.; Zhou, T.; Hosta-Rigau, L.; Sun, Y. One-pot green synthesis of biocompatible graphene quantum dots and their cell uptake studies. *ACS Applied Bio Materials* **2018**, *1* (2), 452-461.
- (73) Noor, N. F. a. M.; Badri, M. A. S.; Salleh, M. M.; Umar, A. A. Synthesis of white fluorescent pyrrolic nitrogen-doped graphene quantum dots. *Optical Materials* **2018**, *83*, 306-314.
- (74) Qin, Y.; Cheng, Y.; Jiang, L.; Jin, X.; Li, M.; Luo, X.; Liao, G.; Wei, T.; Li, Q. Top-down strategy toward versatile graphene quantum dots for organic/inorganic hybrid solar cells. *ACS Sustainable Chemistry & Engineering* **2015**, *3* (4), 637-644.
- (75) Zhao, Y.; Wu, X.; Sun, S.; Ma, L.; Zhang, L.; Lin, H. A facile and high-efficient approach to yellow emissive graphene quantum dots from graphene oxide. *Carbon* **2017**, *124*, 342-347.
- (76) Pan, D.; Zhang, J.; Li, Z.; Wu, M. Hydrothermal route for cutting graphene sheets into blue-luminescent graphene quantum dots. *Advanced materials* **2010**, *22* (6), 734-738.
- (77) Sun, F.; Ghosh, H.; Tan, Z.; Sivoththaman, S. Top-down synthesis and enhancing device adaptability of graphene quantum dots. *Nanotechnology* **2023**, *34* (18), 185601.
- (78) Hasan, M. T.; Lee, B. H.; Lin, C.-W.; McDonald-Boyer, A.; Gonzalez-Rodriguez, R.; Vasireddy, S.; Tsedev, U.; Coffey, J.; Belcher, A. M.; Naumov, A. V. Near-infrared emitting graphene quantum dots synthesized from reduced graphene oxide for in vitro/in vivo/ex vivo bioimaging applications. *2D Materials* **2021**, *8* (3), 035013.
- (79) Ponomarenko, L. A.; Schedin, F.; Katsnelson, M. I.; Yang, R.; Hill, E. W.; Novoselov, K. S.; Geim, A. K. Chaotic Dirac billiard in graphene quantum dots. *Science* **2008**, *320* (5874), 356-358.
- (80) Chua, C. K.; Sofer, Z.; Simek, P.; Jankovsky, O.; Klimova, K.; Bakardjieva, S.; Hrdličková Kučková, S. t. p. n.; Pumera, M. Synthesis of strongly fluorescent graphene quantum dots by cage-opening buckminsterfullerene. *Acs Nano* **2015**, *9* (3), 2548-2555.
- (81) Xie, J.-D.; Lai, G.-W.; Huq, M. M. Hydrothermal route to graphene quantum dots: Effects of precursor and temperature. *Diamond and Related Materials* **2017**, *79*, 112-118.
- (82) Xie, M.; Su, Y.; Lu, X.; Zhang, Y.; Yang, Z.; Zhang, Y. Blue and green photoluminescence graphene quantum dots synthesized from carbon fibers. *Materials Letters* **2013**, *93*, 161-164.
- (83) Umrao, S.; Jang, M.-H.; Oh, J.-H.; Kim, G.; Sahoo, S.; Cho, Y.-H.; Srivastva, A.; Oh, I.-K. Microwave bottom-up route for size-tunable and switchable photoluminescent graphene quantum dots using acetylacetone: New platform for enzyme-free detection of hydrogen peroxide. *Carbon* **2015**, *81*, 514-524.
- (84) Hong, G.-L.; Zhao, H.-L.; Deng, H.-H.; Yang, H.-J.; Peng, H.-P.; Liu, Y.-H.; Chen, W. Fabrication of ultra-small monolayer graphene quantum dots by pyrolysis of trisodium citrate for fluorescent cell imaging. *International journal of nanomedicine* **2018**, 4807-4815.
- (85) Mohanaraman, S. P.; Chidambaram, R. A holistic review on Red Fluorescent Graphene Quantum Dots, its synthesis, unique properties with emphasis on biomedical applications. *Heliyon* **2024**.

- (86) Zeng, Q.; Feng, T.; Tao, S.; Zhu, S.; Yang, B. Precursor-dependent structural diversity in luminescent carbonized polymer dots (CPDs): the nomenclature. *Light: Science & Applications* **2021**, *10* (1), 142.
- (87) Kuo, W.-S.; Shao, Y.-T.; Huang, K.-S.; Chou, T.-M.; Yang, C.-H. Antimicrobial amino-functionalized nitrogen-doped graphene quantum dots for eliminating multidrug-resistant species in dual-modality photodynamic therapy and bioimaging under two-photon excitation. *ACS applied materials & interfaces* **2018**, *10* (17), 14438-14446.
- (88) Wang, L.; Li, W.; Li, M.; Su, Q.; Li, Z.; Pan, D.; Wu, M. Ultrastable amine, sulfo cofunctionalized graphene quantum dots with high two-photon fluorescence for cellular imaging. *ACS Sustainable Chemistry & Engineering* **2018**, *6* (4), 4711-4716.
- (89) Santarelli, G.; Perini, G.; Salustri, A.; Palucci, I.; Rosato, R.; Palmieri, V.; Iacovelli, C.; Bellesi, S.; Sali, M.; Sanguinetti, M. Unraveling the potential of graphene quantum dots against Mycobacterium tuberculosis infection. *Frontiers in Microbiology* **2024**, *15*, 1395815.
- (90) Lakshmanakumar, M.; Nesakumar, N.; Sethuraman, S.; Rajan, K.; Krishnan, U. M.; Rayappan, J. B. B. Functionalized graphene quantum dot interfaced electrochemical detection of cardiac Troponin I: an antibody free approach. *Scientific reports* **2019**, *9* (1), 17348.
- (91) Xiaoyan, Z.; Zhangyi, L.; Zaijun, L. Fabrication of valine-functionalized graphene quantum dots and its use as a novel optical probe for sensitive and selective detection of Hg²⁺. *Spectrochimica Acta Part A: Molecular and Biomolecular Spectroscopy* **2017**, *171*, 415-424.
- (92) Yang, Q.; Duan, J.; Yang, W.; Li, X.; Mo, J.; Yang, P.; Tang, Q. Nitrogen-doped carbon quantum dots from biomass via simple one-pot method and exploration of their application. *Applied Surface Science* **2018**, *434*, 1079-1085.
- (93) Perini, G.; Palmieri, V.; Friggeri, G.; Augello, A.; De Spirito, M.; Papi, M. Carboxylated graphene quantum dots-mediated photothermal therapy enhances drug-membrane permeability, ROS production, and the immune system recruitment on 3D glioblastoma models. *Cancer Nanotechnology* **2023**, *14* (1), 13.
- (94) Zhu, S.; Song, Y.; Wang, J.; Wan, H.; Zhang, Y.; Ning, Y.; Yang, B. Photoluminescence mechanism in graphene quantum dots: Quantum confinement effect and surface/edge state. *Nano Today* **2017**, *13*, 10-14.
- (95) Angl, A.; Sinelnikov, R.; Meldrum, A.; Veinot, J. G.; Balberg, I.; Azulay, D.; Millo, O.; Rieger, B. Photoluminescence through in-gap states in phenylacetylene functionalized silicon nanocrystals. *Nanoscale* **2016**, *8* (15), 7849-7853.
- (96) Setianto, S.; Panatarani, C.; Singh, D.; Joni, I. M. Semi-empirical infrared spectra simulation of pyrene-like molecules insight for simple analysis of functionalization graphene quantum dots. *Scientific Reports* **2023**, *13* (1), 2282.
- (97) Topkiran, U. C.; Valimukhametova, A. R.; Vashani, D.; Paul, H.; Dorsky, A.; Sottile, O.; Johnson, D. A.; Burnett, W.; Coffey, J. L.; Akkaraju, G. R. Holistic Investigation of Graphene Quantum Dot Endocytosis. *Small* **2025**, 2406095.
- (98) Lingegowda, D. C.; Kumar, J. K.; Prasad, A.; Zarei, M.; Gopal, S. FTIR spectroscopic studies on cleome gynandra-Comparative analysis of functional group before and after extraction. *Rom. J. Biophys* **2012**, *22* (3-4), 137-143.
- (99) Rasheed, P. A.; Ankitha, M.; Pillai, V. K.; Alwarappan, S. Graphene quantum dots for biosensing and bioimaging. *RSC advances* **2024**, *14* (23), 16001-16023.
- (100) Nassar, A. M.; Ahmed, N. S.; Haseeb, M. E.; Abdel-Rahman, A. A.-H.; Nasser, R. M. SYNTHESIS AND EVALUATION OF TERPOLYMERS AS VISCOSITY INDEX IMPROVERS AND POUR POINT DEPRESSANTS. *Petroleum & Coal* **2017**, *59* (4).
- (101) Shang, J.; Ma, L.; Li, J.; Ai, W.; Yu, T.; Gurzadyan, G. G. The origin of fluorescence from graphene oxide. *Scientific reports* **2012**, *2* (1), 792.
- (102) Tian, P.; Tang, L.; Teng, K.; Lau, S. Graphene quantum dots from chemistry to applications. *Materials today chemistry* **2018**, *10*, 221-258.

- (103) Teraphongphom, N.; Kong, C. S.; Warram, J. M.; Rosenthal, E. L. Specimen mapping in head and neck cancer using fluorescence imaging. *Laryngoscope investigative otolaryngology* **2017**, *2* (6), 447-452.
- (104) Valimukhametova, A. R.; Fannon, O.; Topkiran, U. C.; Dorsky, A.; Sottile, O.; Gonzalez-Rodriguez, R.; Coffey, J.; Naumov, A. V. Five near-infrared-emissive graphene quantum dots for multiplex bioimaging. *2D Materials* **2024**, *11* (2), 025009.
- (105) Qi, L.; Pan, T.; Ou, L.; Ye, Z.; Yu, C.; Bao, B.; Wu, Z.; Cao, D.; Dai, L. Biocompatible nucleus-targeted graphene quantum dots for selective killing of cancer cells via DNA damage. *Communications biology* **2021**, *4* (1), 214.
- (106) Galande, C.; Mohite, A. D.; Naumov, A. V.; Gao, W.; Ci, L.; Ajayan, A.; Gao, H.; Srivastava, A.; Weisman, R. B.; Ajayan, P. M. Quasi-molecular fluorescence from graphene oxide. *Scientific reports* **2011**, *1* (1), 85.